agriculture

MDPI

Article

Design and Experiment of Bionic Film-Lifting Shovel for Residual Film Recycling Machine

Yan Zhao [1,2], Wenzhe Wang [1,2], Haojun Wen [1,2], Xuegeng Chen [1,2], Xinliang Tian [1,2,*], Yuanchao Li [1,2] and Guangliang Huang [1,2]

[1] College of Mechanical and Electrical Engineering, Shihezi University, Shihezi 832000, China; zhaoyan@shzu.edu.cn (Y.Z.); 13109876683@163.com (W.W.); wenhaojun1@xjshzu.com (H.W.); chenxg130@sina.com (X.C.); liyuanchao@stu.shzu.edu.cn (Y.L.); huangguangliang@stu.shzu.edu.cn (G.H.)
[2] Key Laboratory of Northwest Agricultural Equipment, Ministry of Agriculture and Rural Affairs, Shihezi 832000, China
* Correspondence: txlshzu0326@163.com

Abstract

The aim of this study is to improve the film removal rate of a film removal device on a residual film recovery machine and mitigate the soil compaction caused by film removal operations during the residual film recovery process. We designed a bionic film-lifting shovel by applying the contour curve of the first claw of the North China mole cricket's front foot to the soil-penetrating portion of the film-lifting tines. Based on agronomic requirements and mechanical analysis of the operation process, the biomimetic blade was developed to break up soil more effectively and lift the residual film more efficiently. The contour features were obtained using high-definition cameras, with the fitting equation guiding the design of the soil-penetrating structure. A three-dimensional model was constructed using SolidWorks. Tensile tests provided the physical parameters of the autumn residual film, enabling the creation of a finite element model using the Mohr–Coulomb yield criterion. Simulation comparisons showed that the biomimetic shovel teeth reduced the operating resistance by 9.3% compared to conventional teeth. Soil trench experiments validated these results, demonstrating a 4.24% higher film-lifting rate and average resistance of 411.49 N for the bionic shovel versus 454.70 N for the conventional one. The close match between the experimental and simulation results confirms the effectiveness of the bionic design in meeting the resistance reduction requirements.

Keywords: residual film recovery; film-lifting blade; bionics; finite element analysis; soil bin test

check for updates

Academic Editor: Bruno Bernardi

Received: 1 October 2025
Revised: 20 October 2025
Accepted: 24 October 2025
Published: 30 October 2025

Citation: Zhao, Y.; Wang, W.; Wen, H.; Chen, X.; Tian, X.; Li, Y.; Huang, G. Design and Experiment of Bionic Film-Lifting Shovel for Residual Film Recycling Machine. *Agriculture* **2025**, *15*, 2260. https://doi.org/10.3390/agriculture15212260

Copyright: © 2025 by the authors. Licensee MDPI, Basel, Switzerland. This article is an open access article distributed under the terms and conditions of the Creative Commons Attribution (CC BY) license (https://creativecommons.org/licenses/by/4.0/).

1. Introduction

Plastic film mulching cultivation has the function of increasing temperature, preserving soil moisture, suppressing weeds, promoting crop root development and improving crop quality [1]. The main material of agricultural land film is polyethylene, and the degradation time in natural conditions is 200–400 years [2]. Due to the insufficient recovery of the plastic film, the amount of residual plastic film in the soil continues to increase, which is not conducive to the absorption of water and crop nutrients and affects the crop yield [3,4]. At present, the mechanized recovery of the residual film is an effective method to deal with the residual soil film, in which the film is an important part of the process of the residual film recovery machine [5].

The film-lifting device is the main actuator of the film-lifting operation within the residual film recovery machine. The film-lifting shovel is the main component of the film-lifting device, and its performance critically affects the surface residual film recovery rate and operational energy consumption. This is because an insufficient operating depth prevents the shovel from penetrating beneath the film, leaving covered plastic uncollected, while an excessive depth significantly increases the power demand of the machine. In order to improve the efficiency of the residual film recovery machine, the structure optimization of the film shovel is one of the key points in residual film recovery. Kang Jianming [6] designed a parabolic guide curve film shovel, where the film shovel spacing is 220 mm, the operating speed is 10 m/s, and the theoretical film rate can reach 93.8% when the earth angle is 30. Yang Songmei [7] conducted a univariate field test with three initiation teeth structures as the variable, which proved that the structure of the initiation teeth had a significant impact on the initiation rate and resistance.

In recent years, the application of bionics in soil parts has continued to increase, which effectively alleviates the soil resistance problem in the operation process of soil parts [8]. Wang Jinwu [9] studied the streamline curve of the sturgeon body and designed a bionic fertilization furrow opener with the characteristic curve structure of the sturgeon body. The experimental results showed that the furrow resistance and soil disturbance were smaller compared with the ordinary fertilization furrow opener. Li Junwei [10] studied the leaf sheath structure of a grass root film and designed a potato-digging shovel with a bionic ripple structure. Field experiments showed that the unit fuel consumption of the bionic longitudinal ripple shovel was reduced by 17.15% and the resistance by 14.45% compared with an ordinary plain shovel.

In conclusion, the key factor affecting the film-lifting performance of the residual film recovery machine is the film shovel structure, and the application of bionic technology in the design of soil parts can effectively improve the resistance reduction performance of soil parts. In this study, the biomimetic design concept and finite element method are applied to simulate the method's equation for the design of the soil surface. With the surface residual film as the test material, a tensile test was carried out, the material characteristic parameters were obtained, the multi-soil finite element composite model was created, and the film process and resistance of the bionic shovel and ordinary shovel were dynamically simulated using LS-DYNA. The soil tank test was carried out to verify the simulation results, and the resistance reduction performance and film-lifting effect of the bionic film shovel were tested, so as to provide a reference for the design of the film-lifting device and earth parts of the residual film recovery machine.

2. Bionic Film Shovel Design

2.1. Extraction and Fitting of Contour Curve of First Paw Toe of North China Mole Crickets

The North China mole cricket mainly lives in sandy soil, as shown in Figure 1, living in caves excavated by its own forefoot, an insect that can be quickly excavated in sandy soil, after hundreds of years of natural evolution and selection. The front foot of the North China mole cricket have a huge advantage in the process of sand mining [11,12]. The main cause of the strong soil excavation performance of the mole cricket in North China is that the structural contour of its paw toe can effectively break the soil and reduce resistance in the process of soil excavation [13]. The configuration characteristics of the cross-section of the mole cricket in North China play a major role in reducing the cutting resistance [14], and the size ratio of the first toe contour of the forefoot is more similar to that of the film shovel. Therefore, the contour curve of the first toe of the mole cricket in North China is investigated in this study. There are some differences in the inner and outer contour of the toe; the inner side of the toe lands earlier and more directly contacts the soil. Therefore,

the contour of the first toe is divided into inner and outer parts, and the fitting equation is obtained.

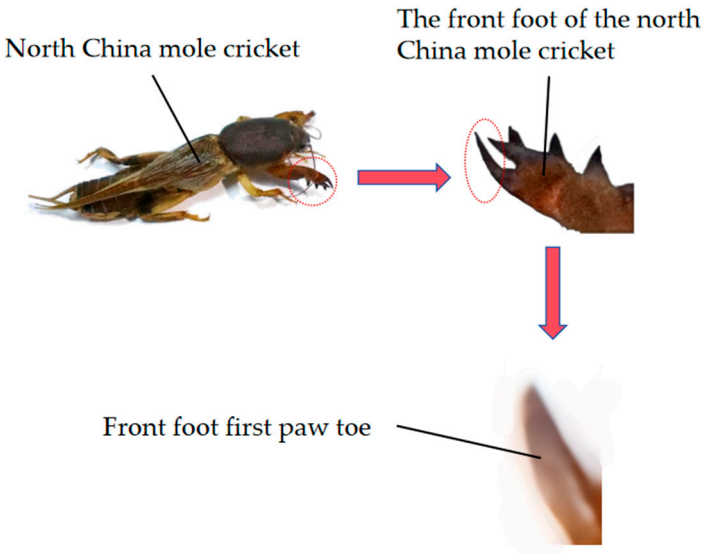


Figure 1. The structure of north China mole cricke.

Using an HD camera to ascertain the structure of the first paw information acquisition, image processing software to obtain the two-dimensional contour curve [15], then adding the two-dimensional contour curve into AutoCAD 2024 to give the transverse and vertical coordinate value [16,17], the coordinate data are input into the data processing software ORIGIN, 2024 and we draw the outline of the peak fitting using the data analysis tool for two sets of scatter plot fitting analysis, as shown in Figure 2. The first paw before and after the contour fitting equation is represented by the Gaussian equation.

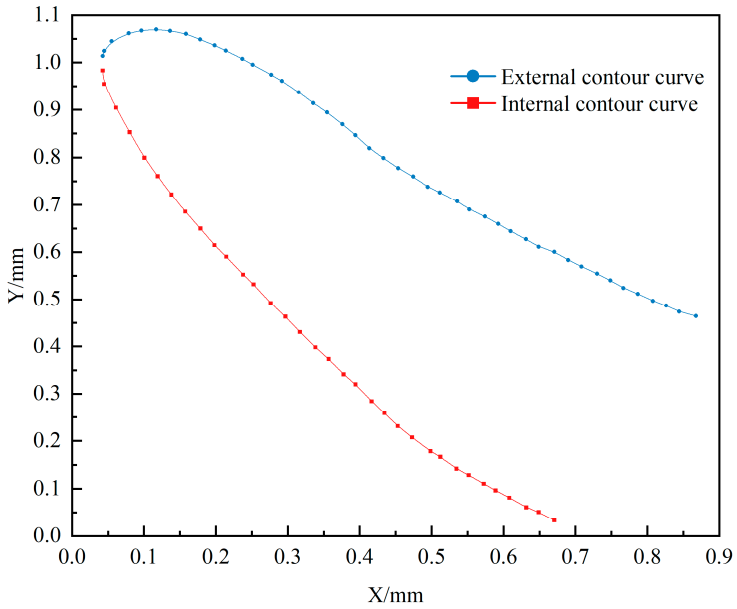


Figure 2. The inner and exter contour of the first toe of north China mole cricket.

The Gaussian equation for the front and back outline of the first paw of the mole cricket is as follows:

$$f(x) = a_1 e^{-\left(\frac{x-b_1}{c_1}\right)^2} + a_2 e^{-\left(\frac{x-b_2}{c_2}\right)^2} \quad (1)$$

x—position coordinate along the characteristic direction of the claw toe, mm; a_1—amplitude of the first Gaussian component of the inner (outer) contour of the first claw toe, mm; a_2—amplitude of the second Gaussian component of the inner (outer) contour of the first claw toe, mm; b_1—peak center position of the first Gaussian component of the inner (outer) contour of the first claw toe, mm; b_2—peak center position of the second Gaussian component of the inner (outer) contour of the first claw toe, mm; c_1—width parameter of the first Gaussian component of the inner (outer) contour of the first claw toe, mm; c_2—width parameter of the second Gaussian component of the inner (outer) contour of the first claw toe, mm; e—natural constant (base of the exponential function), dimensionless.

In the process of digging, the first toe of the North China mole cricket has extension and outward expansion [18], and the form of extended movement is similar to that of film movement. The extended motion process is associated with the characteristic structure of the paw toe cross-section, and the paw toe contour fitting equation can be used to describe the characteristics of the cross-section. In conclusion, the fitting curve equation of the first claw toe of the North China mole cricket shown in Table 1 and Equation (1) can be used as the design basis for the bionic film shovel tooth.

Table 1. The coefficient of curve equation to the first toe of north China mole cricket.

Ratio	Inner Contour of the First Paw Toe	Outer Contour of the First Paw Toe
a_1	0.126	2062.908
b_1	0.464	0.32721
c_1	0.0635	−0.759
a_2	0.146	−2.811
b_2	0.656	1.278
c_2	0.465	−2.755
SSE	1.742	6.574
R^2	0.99959	0.99927

2.2. Design Principle and Process

The film shovel used in the residual film recovery machine mainly includes the bullet tooth, shovel sieve, tooth and other types [19]. This study is based on the design of the tooth film shovel. Usually, the main working part of the tooth-type film shovel is the shovel tooth, as shown in Figure 3, which can be simply divided into three parts: connection, transition and earth. The soil part of the shovel should have the ability to break the soil and turn out the surface film. During operation, the tractor pulls the residual film recovery machine forward, allowing the film-lifting shovel to slide beneath the mulched soil under the combined action of its own weight and soil-entry angle. A four-bar linkage mechanism regulates the penetration depth of the shovel and enables it to follow ground contours. As the shovel enters the soil, it lifts the soil layer containing the residual film. Subsequently, spring-loaded film-picking teeth engage and lift the film upward. Finally, the film is scraped off into the collection box by the film-removal device. Therefore, the soil resistance and the film performance [20] should be considered in the design of the shovel part.

Based on the above findings, the contour curve of the first toe of the North China mole cricket's forefoot is more consistent with the guide surface of the shovel tooth, so that the surface residual film can be gently moved to the transition part during the operation of the residual film recovery machine. In the process of operation, the soil can easily accumulate before the shovel, resulting in the concentration of resistance in the mining process and the poor effect of the soil crushing. The structure of the mole cricket can slide the soil during the excavation to reduce resistance and slow down the effect of choking. So, with reference to the contour structure of the North China mole cricket claw toe, the application of the North China mole cricket front foot means that the first toe of the internal and external outline

fitting equation is used to design the film shovel part, guiding the surface curve, combined with the design of the film shovel reference size, to determine the length of the fitting curve, but we also want to balance the film shovel operation required for film performance.

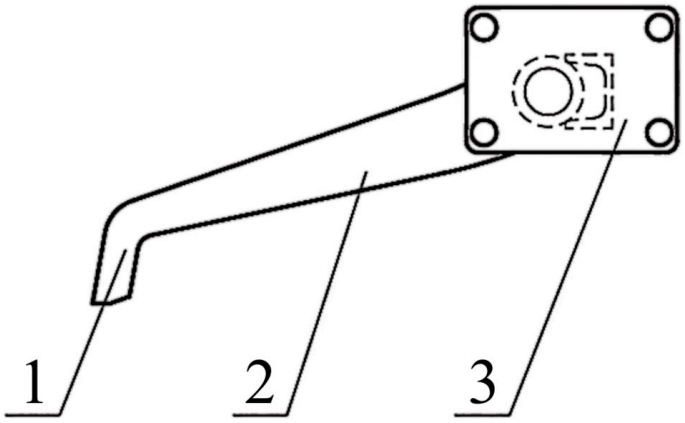


Figure 3. Ted film shovel 1. Earth-entering section, 2. Transition section, 3. Connecting part.

2.3. Force Analysis of Bionic Film Shovel

During the operation of the film-lifting shovel, the resistance is influenced by the shovel's geometry, penetration depth, and soil engagement angle. Under the combined effect of these resistive forces, the power consumed to overcome soil-related resistance accounts for approximately 65% of the total operational power consumption of the film-lifting shovel [21]. The degree of soil crushing depends on the structure of the soil surface, the displacement of the soil and the film after the force; further, the soil and the film form the adhesion and friction of the tooth surface. The purpose of the film shovel operation is to overcome the bond between the plastic film and soil, and this promotes the relative motion of the plastic film and soil. Therefore, it is necessary to establish a mechanical model of the film shovel tooth surface and analyze the source of resistance of the film shovel. The lateral mechanical balance equation is derived from Figure 4.

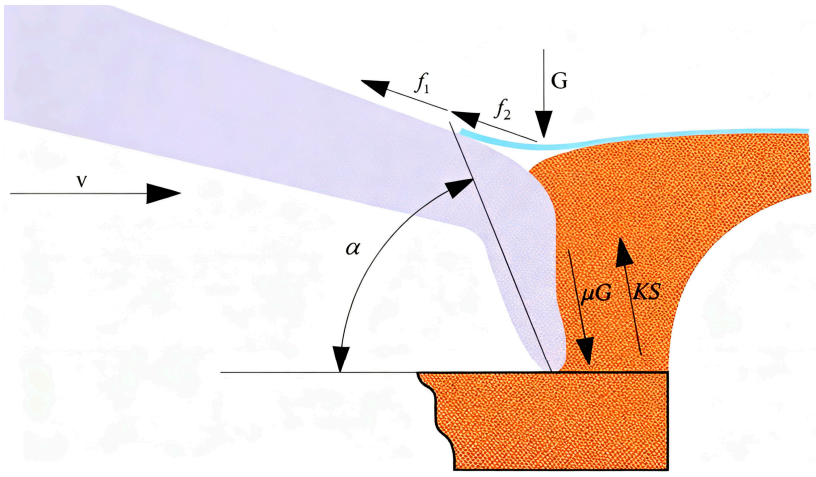


Figure 4. Analysis of lateral force.

The lateral mechanical balance equation is derived from Figure 4:

$$F = \mathrm{G}\sin\alpha + (\mu \mathrm{G} + KS + f_1 + f_2)\cos\alpha \quad (2)$$

F—gravity of the film soil mixture above the film shovel, N; G—gravity of the film soil mixture above the film shovel, N; α—penetrating angle, °; K—soil adhesion, MPa;

S—operating contact area, mm^2; f_1—the friction between the film shovel and the film, N; f_2—the friction between the film shovel and the film, N; μ—friction factor within the soil.

Regarding the mixture of film soil above the shovel, the horizontal force equation is as follows:

$$G_n \cos\beta + (KS + f_1 + f_2 + \mu G_n)\cos\alpha + KS\sin\beta - G_t\cos\alpha - \mu G_n\cos\beta = 0 \quad (3)$$

Regarding the mixture of film soil above the shovel, the horizontal force equation is as follows:

$$G + (\mu G_n + KS + f_1 + f_2)\sin\alpha + KS\cos\beta + \mu G_n\sin\alpha - G_n\sin\beta = 0 \quad (4)$$

G_n—starting film shovel normal load, N; G_t—lateral load of film shovel, N; β—anterior failure inclination (°).

The vertical force equation can be seen in Equations (2)–(4):

$$F = \frac{G}{Z} + \frac{KS + f}{Z(\sin\beta + \mu\cos\beta)} + \frac{KS + f}{Z(\sin\beta + \mu\cos\beta)} \quad (5)$$

μ_1—soil and metal friction factor; h—excavating depth, mm; Z—constant.

According to the mechanical model and force analysis of the shovel and the mixture in the process, the structure parameters, the soil physical characteristic parameters and the working condition parameters are the main factors affecting the resistance of the shovel.

$$\begin{cases} \frac{\partial F}{\partial \alpha} = \frac{-(KS+f_1 l+f_2 l)}{(\cos\alpha-\sin\alpha)^2}(\cos\alpha - \sin\alpha) = 0 \\ \frac{\partial F}{\partial \beta} = \frac{-(KS+f_1 l+f_2 l)}{(\sin\beta-\sin\alpha)^2}(\cos\beta - \sin\beta) = 0 \\ \left(0 \le \alpha \le \frac{\pi}{2}, 0 \le \beta \le \frac{\pi}{2}\right) \end{cases} \quad (6)$$

According to the multiple derivative analysis, the inlet angle α and the resistance angle β are smaller when the angle is closer to 45. The range of the soil angle α is 22–33°, and the resistance angle β is 28–35°. The soil angle is too large, which can cause choking, increasing energy consumption, and the angle of the soil is too small, which affects the film performance of the film shovel. Combined with [22,23], the entry angle of the film shovel is generally 10–35°, and the entry angle of the bionic film shovel is 30°.

3. FEM Simulative Analysis

The finite element software ANSYS 2024/LS-DYNA R14.0 is used to simulate the operation process of the ordinary and bionic film shovels and to compare the working resistance and film conditions of the two film shovels.

3.1. Simulation Model Parameter Setting

3.1.1. Surface Residual Film Model

In order to determine the elastic modulus parameters of the surface residues, the autumn field surface residues with 0.01 mm thickness collected from Liangli Village, Laojie Street, Shihezi City (latitude 44.32253201° N, longitude 85.99529472° E), were selected as the experimental object, and 10 surface residues with size (length and width) of 150 mm and 10 mm were made and marked [24], as shown in Figure 5. Tensile tests were conducted using an INSTRON E1000 (Instron, High Wycombe, UK) universal testing machine to obtain the maximum tensile load of the surface film sample, as shown in Figure 6. The tensile length at fracture and the elastic modulus parameters are shown in Table 2. During the experiment, the sample surface was kept perpendicular to the ground, the laboratory temperature was (26 ± 2) °C, and the tensile speed was set at 60 mm/min [25].

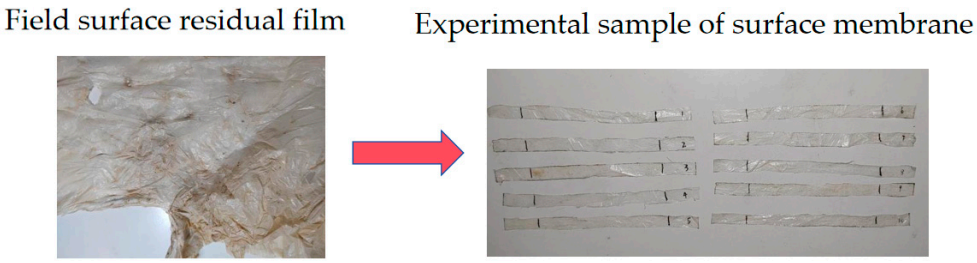


Figure 5. Preparation of surface residual film test samples.



Figure 6. The intelligent control electronic universal tester conducts tensile test on the sample.

Table 2. Tensile data of surface film specimens.

Sample Number	Breaking and Tensile Load/N	Break and Tensile Length/mm	Modulus of Elasticity/MPa
1	4.38	62.40	105.29
2	5.32	56.75	140.62
3	4.55	47.26	144.41
4	7.23	55.58	195.12
5	5.93	81.13	109.64
6	6.88	73.52	140.37
7	4.56	57.37	119.23
8	8.22	65.44	188.42
9	5.24	41.25	190.55
10	3.98	39.19	152.33
average value	5.63	57.99	148.60
standard deviation	1.40	13.37	33.21

To simplify the operation, the surface residual film model is set to the Shell cell, and the elastic modulus parameter applies the average of the tensile experimental data. In the process of bionic film shoveling, it is assumed that the residual film of the cotton field is spread on the surface after the autumn, the residual film is regarded as static, and the fluctuation in the process of the film shoveling is ignored. The elastic modulus parameters of the surface residual film model refer to the mean data of the residual film tensile test. The other main parameters are obtained according to the study in [26]. All the main parameters

are shown in Table 3, and the default value of the material model MAT 3 is selected for the other parameters.

Table 3. Main material physical parameters of surface residual film.

Parameters	Values
Surface residual film density/(g·mm^{-3})	0.00092
Elastic modulus/MPa	148.6
Poisson's ratio	0.4

3.1.2. Soil Model

In the LS-DYNA finite element simulation, the MAT_FHWA_SOIL soil material model of the Mohr–Coulomb yield criterion is described in Formula (7) [27].

$$F = -p\sin\varphi + \sqrt{J_2K(\theta)^2 + \partial^2\sin^2\varphi} - c\cos\varphi = 0 \quad (7)$$

F—model to yield the surface force, N; p—pressure, N; φ—the internal friction angle, °; J_2—the second invariant of the stress bias tension; $K(\theta)$—the stress rod angle function; c—the cohesive force, N; α—the parameter defining the closeness between the corrected yield surface and the standard Mohr–Coulomb yield surface.

In combination with the soil characteristics of the Xinjiang cotton field area, the main parameters of the soil model are given [28,29], as shown in Table 4. Since there is no material model MAT_147 in ANSYS/LS-DYNA, the post-processing software LS-PREPOST 5.2.0. is required to set the material model in the K file as MAT_147 and modify the main parameters, and the remaining parameters should be set according to the default value of the MAT_FHWA_SOIL material model. The soil model was a cuboid with a structure size of 170 mm × 110 mm × 105 mm, modeled by SolidWorks, stored in IGES format and imported into ANSYS/LS-DYNA.

Table 4. Main material physical parameters of soil.

Parameters	Values
Soil density/(g·mm^{-3})	0.0015
Specific density of solid particles	2.7
Bulk modulus/MPa	28
Shear modulus/MPa	4.5
Cohesive force/MPa	0.01
Internal friction angle/rad	0.532
Moisture capacity/%	25
Water density/(g·mm^{-3})	0.001

3.1.3. Film-Lifting Shovel Tooth Model

The film shovel tooth is modeled by the 3D software SolidWorks 2024, stored as IGES format into ANSYS; the shovel tooth is defined as the Solid164 solid unit, and the material of the shovel tooth model is set as the rigid body material model MAT_RIGID [30]. The main parameters of the model material are shown in Table 5.

Table 5. Main material physical parameters of the shovel teeth model.

Parameters	Values
Density of shovel teeth/(g·mm^{-3})	0.00786
Elastic modulus/MPa	1.92
Poisson's ratio	0.3

3.2. Simulation Process and Result Analysis of Film-Lifting Operation

At present, most film-lifting devices of residual film recovery machines adopt the tooth-type shovel structure. The conventional tooth-type film shovel is simple to manufacture and demonstrates robust soil-breaking capability. The simulation tests were primarily conducted to explore the advantages of the bionic shovel tooth structure; hence, a comparative study was carried out between the bionic and conventional film shovels. To minimize experimental error, the model dimensions of the bionic shovel teeth were maintained nearly identical to those of the conventional shovel. Meanwhile, the contact types between the two shovels and the soil residual film models were defined as ERODING_SINGLE_SURFACE, encompassing all surface definitions and contact configurations. The soil model was fully constrained around its periphery. The soil and residual film models were treated as infinite in size, with non-reflective boundary constraints [31,32] applied to their surrounding boundaries.

3.2.1. Contrast Experiment of the Film Initiation Process

A simulation comparison experiment was carried out to simulate the film-lifting process of the two kinds of shovels. According to the operating parameters of the residual film recovery machine, the advance speed of the two types of shovels was set to 1.67 m/s, the soil depth was controlled at 80 mm, the soil angle was 30, the duration was 0.1 s, and the total simulation duration was 0.1s [33]. The simulation results were observed and compared, as shown in Figure 7.

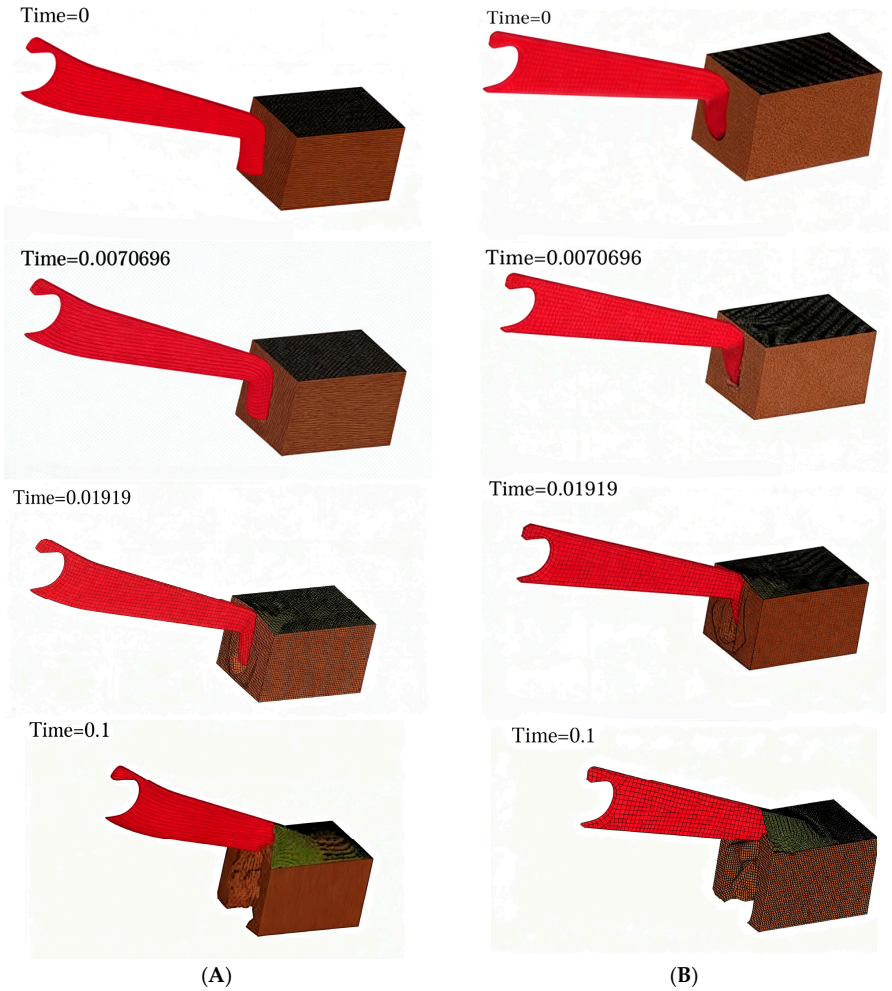


Figure 7. Process diagram of film operation. (**A**) Simulation of conventional film-lifting shovel tooth. (**B**) Simulation of bionic film-lifting shovel tooth.

Along with the movement, the shovel tooth tip comes into contact with the soil. When the shovel tooth enters the soil completely, the soil and the soil unit continue to move upward on the surface of the shovel tooth, some soil units will be further impacted and begin to distort, and the surface residual will continue to move upward along the shovel tooth. Compared with ordinary shovels, the disturbance and crushing effect of the soil unit around the bionic shovels is better, and the choking phenomenon is relatively reduced, which indirectly reduces the resistance of film operation.

3.2.2. Comparison of Film Resistance

According to Formula (4), the resistance is mainly influenced by the structure parameters, soil physical characteristics and working condition parameters, the resistance of the LS-DYNA R14.0 post-processing software, the LS-PREPOST 4.8.0, and the resistance value curve of 0–0.1s, which is imported into Origin2024, as shown in Figure 8.

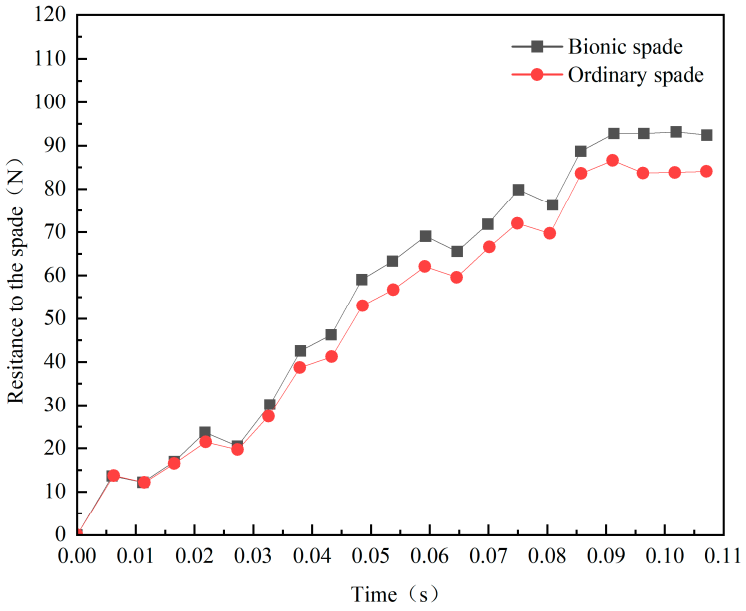


Figure 8. Simulated Resistance Comparison between Bionic and Conventional Film-Lifting Shovels.

At 0.005 s, the film resistance starts at 0.02 s. The resistance of the film increases significantly and reaches 88.45 N. At the maximum resistance value at 0.08 s, the resistance value reaches the maximum of 80.23 N at 0.085 s. In comparison, the resistance reduction rate of the bionic film shovel is 9.3%.

4. Indoor Soil Bin Experiment

4.1. Experimental Conditions and the Equipment

The soil bin test for both the bionic and conventional toothed film-lifting shovels was conducted at the Practical Center of the North Garden New Area of Shihezi University, using a soil bin test bench as the main experimental apparatus. The main components include the test bench vehicle, a three-directional mechanical sensor and data acquisition system, a three-point hitch mechanism, a film-lifting shovel connecting frame, depth-limiting rollers, and soil for experiments. The film-lifting shovel connecting frame was attached to the three-point hitch mechanism using U-bolts. Two sets of film-lifting shovels were securely fixed to the frame with bolts, enabling easy disassembly. The depth of penetration of the film-lifting shovels is adjusted by the depth-limiting rollers and adjusting plates installed on the connecting frame to ensure the required depth for the experiment. The three-directional mechanical sensor is installed at the junction of the upper and lower layers of the three-

point hitch mechanism, and the depth of the soil layer for the experimental soil is ensured to be at least 300 mm, as shown in Figure 9.

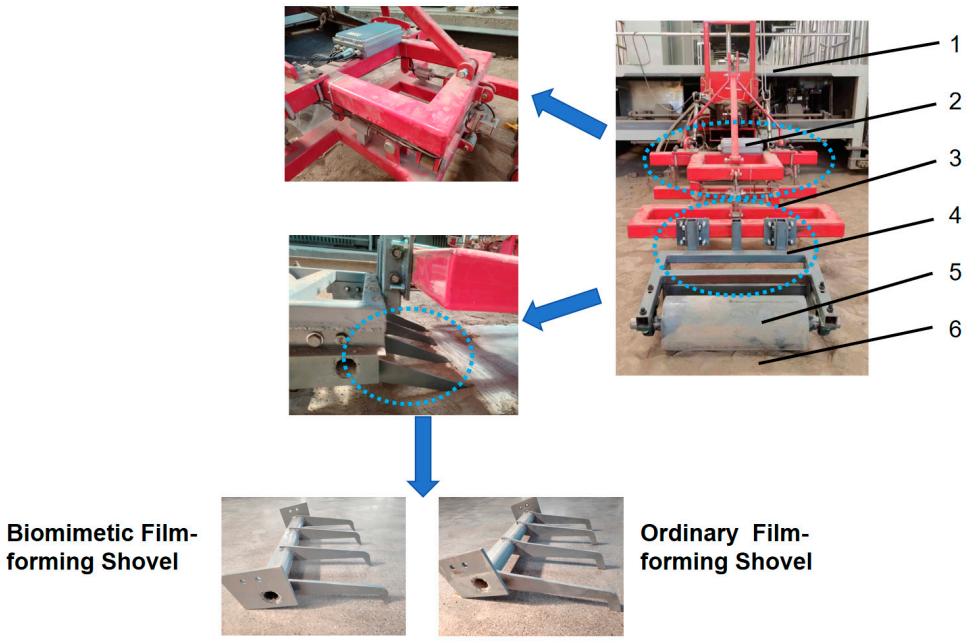


Figure 9. Schematic diagram of the soil bin test bench. 1. Test bench cart. 2. Triaxial mechanical sensor and data acquisition system. 3. Three-point suspension mechanism. 4. Film-lifting shovel connecting frame. 5. Depth-limiting roller. 6. Soil for experiments.

The soil bin experimental trolley has a speed adjustment range of 1 to 2000 mm/s, with an adjustment accuracy of 1 mm/s. The operation process of the two types of film-lifting shovels is recorded in real time using high-definition video equipment. During the soil bin experiment, the resistance encountered by the film-lifting shovels is measured in real time through a three-axis force sensor and the experimental trolley data acquisition system. The measurement range of the sensor is 1 to 2000 N, with a precision of 1 N, and the data acquisition frequency is 50 times/s.

To further ensure that the soil bin experiment is consistent with actual field conditions, the experimental soil was taken from a cotton field in Shihezi City, Xinjiang, China. Before the start of the soil bin experiment, the experimental area was set to a length of 5 m and a width of 1.3 m. The experimental soil was processed by watering, breaking up the soil, and compacting it in sequence. Following the actual conditions of the field surface in autumn, a 1 m wide strip of residual film from the soil surface was laid out and compacted over the experimental area. The working speed of the experimental trolley was set to 1.67 m/s, the depth of the film-lifting shovels into the soil was set to 80 mm, and the angle of entry was set at 30 degrees, with an operation time of 2 s.

4.2. Soil Bin Test

4.2.1. Work Effect Comparison Test

Usually, the operation effect of the film-lifting device can be directly reflected by the film-lifting rate [26]. In order to verify the operation effect of the bionic film shovel, 10 groups of film initiation tests were tested on two different shovels on the test platform with the surface residual film, and the film initiation rate of the two kinds of shovels was obtained, as shown in Table 6.

Table 6. The operation conditions of two types of film applicators.

	Biomimetic Film-Lifting Shovel	Conventional Film-Lifting Shovel
Homework situation		
Post-washed picked-up residual film		

A comparative analysis was conducted on the operational effects of two types of soil film-lifting shovels in a soil bin test. The soil heaping observed during the operation of the biomimetic film-lifting shovel was alleviated compared to that of the conventional film-lifting shovel, demonstrating that the biomimetic shovel has superior performance in reducing soil heaping and causes relatively less soil disturbance, which is consistent with the results of finite element simulation tests.

After each set of film-lifting operations is completed, collect the residual film lifted by the film lifter and the non-lifted film left on the ground separately. Package the residual film obtained from each set of experiments. After the experiment, wash the film to remove soil and other impurities and then weigh it. The obtained residual film-quality data are input into Formula (8) to calculate the film-lifting rate. As shown in Table 7, the average film-lifting rate of the biomimetic film lifter is 94.02%, which is 4.24% higher than the average film-lifting rate of the conventional film lifter. The film-lifting efficiency of the biomimetic film lifter was higher than that of the conventional film lifter.

$$\psi = \frac{M_b}{M_a + M_b} \tag{8}$$

ψ—Peeling rate, %.
M_b—Quality of the mulch film not yet lifted by the mulch lifter, kg.
M_a—Quality of the film lifted by the film lifter, kg.

Table 7. Data on the blistering rate of two types of blistering spatulas.

Experiment Number	Biomimetic Film Removal Rate/%	Conventional Film-Lifting Shovel Film Removal Rate/%
1	92.3	87.5
2	94.4	88.2

Table 7. *Cont.*

Experiment Number	Biomimetic Film Removal Rate/%	Conventional Film-Lifting Shovel Film Removal Rate/%
3	95.1	91.4
4	93.7	88.8
5	96.2	91.8
6	93.3	90.5
7	95.3	88.9
8	92.9	90.1
9	92.4	89.9
10	94.6	90.7
mean value	94.02	89.78
standard deviation	1.31	1.40

4.2.2. Film-Lifting Resistance Comparison Test

The peak resistance of the film shovel in the X direction is obtained through the three-direction force sensor and the test bench data acquisition system, and the resistance data of 10 groups of film tests were obtained under the same conditions. During operation, the data acquisition system of the test bench recorded the variation in film resistance over time for different shovel types. The obtained resistance mean values and drag reduction rates for each set of experiments are shown in Table 8.

Table 8. The drag resistance and drag reduction rate of types of film-lifting shovels.

Test Serial Number	Biraised Film Resistance/N	Common Film Shovel Film Resistance/N	Drag Reduction Efficiency/%
1	407.42	445.04	8.45
2	412.90	458.65	9.98
3	405.90	444.42	8.67
4	420.04	453.38	7.35
5	412.66	450.58	8.42
6	408.86	457.67	10.66
7	413.05	449.10	8.03
8	415.06	464.44	10.63
9	404.88	455.30	11.07
10	414.10	464.39	10.83
mean value	411.49	454.70	9.50
standard deviation	4.68	7.16	1.36

5. Conclusions

(1) To address high resistance and soil blockage during residual film recovery, this study analyzed the soil-digging features of mole crickets. The contour of the first claw was captured using high-definition cameras and mathematically represented by a fitted curve. This equation was applied to design the soil-penetrating segment of the bionic film-lifting shovel teeth. A mechanical model of the shovel teeth interacting with the film-soil mixture was established and analyzed to define the structural parameters. Finally, a 3D model of the bionic shovel was constructed in SolidWorks 2024.

(2) Through LS-DYNA dynamic simulation comparisons, it was demonstrated that soil units undergo compression-induced deformation followed by accelerated displacement and eventual fragmentation around the shovel teeth. The bionic blade design facilitated rapid soil fragmentation and promoted guided flow along the tooth surface, effectively reducing soil-blade adhesion and friction. This mechanism enhanced soil flowability

and improved structural drainage efficiency. Consequently, the bionic film-lifting shovel transported fewer soil particles, significantly alleviating soil accumulation and reducing operational resistance by an average of 9.3%. Furthermore, the improved soil handling characteristics minimized root burial during excavation, thereby facilitating subsequent root screening processes.

(3) Soil trench tests were conducted to compare the film-forming effects of two types of shovel teeth. The results showed that the soil accumulation phenomenon and film-forming resistance generated by the biomimetic shovel teeth during simulation tests were significantly better than those generated by conventional shovel teeth. Film-forming resistance was measured using a triaxial force sensor and it was found that the average resistance of the biomimetic blades was 411.49 N, compared to 454.70 N for conventional blades, representing a reduction of 9.5%. This is nearly identical to the 9.3% reduction observed in the simulation test, confirming the reliability of the established LS-DYNA model. The biomimetic film-forming blades had an average film lifting rate of 94.02%, which was 4.24% higher than that of conventional blades. The film-forming efficiency of the biomimetic scraper was higher than that of the conventional scraper. The biomimetic film-forming scraper's structural design is reasonable and meets the drag reduction requirements for film-forming operations involving residual film recovery.

Author Contributions: Conceptualization, Y.L.; methodology, X.C. and H.W.; software, X.T. and W.W.; validation, X.T. and G.H.; writing—original draft preparation, Y.Z. and Y.L.; writing—review and editing, Y.Z. and W.W.; supervision, X.C. and H.W.; funding acquisition, H.W. and X.T. All authors have read and agreed to the published version of the manuscript.

Funding: This research was supported by the Science and Technology Program of XPCC (2024DA023), the Science and Technology Innovation Talent Program (2023CB008-09), the Xinjiang Uygur Autonomous Region Tianchi Talent Project (CZ002549), the Shihezi University Youth Innovation Incuba-tion Talent Program Project (CXPY202321), and the Youth Project of the Excellence Support Pro-gram of Xinjiang Production and Construction Corps (CZ002528).

Institutional Review Board Statement: Not applicable.

Data Availability Statement: The data presented in this study are available on request from the corresponding author.

Conflicts of Interest: The authors declare no conflicts of interest.

References

1. Zhao, Y.; Zheng, X.; Chen, X.G.; Niu, Q.; Ji, C.; Zhou, D.X. Design and test of CMJY-1500 type plastic film residue collecting and balling machine. *Trans. Chin. Soc. Agric. Eng.* **2017**, *33*, 1–9. (In Chinese) [CrossRef]
2. Xu, Y.M.; Fang, S.J.; Ma, X.P.; Zhu, Q.Q. Prevention and Control Strategy for the Pollution of Agricultural Plastic Film. *Strateg. Study CAE* **2018**, *20*, 96–102. [CrossRef]
3. Zhao, Y.; Chen, X.G.; Wen, H.J.; Zheng, X.; Niu, Q.; Kang, J.M. Research Status and Prospect of Control Technology for Residual Plastic Film Pollution in Farmland. *Trans. Chin. Soc. Agric. Mach.* **2017**, *48*, 1–14. (In Chinese) [CrossRef]
4. Wen, H.J.; Chen, X.G.; Cheng, H.; Gou, H.X. Application status and development of farmland mulch recycling machinery. *Trans. Chin. Soc. Agro-Environ. Sci.* **2024**, *43*, 1271–1277. (In Chinese) [CrossRef]
5. Liu, C.; Hu, B.; Luo, X.; Guo, M.Y.; Li, Z.Y.; He, Z.X.; Ghen, Z.L.; Xie, Y.Y. Design and test of residual film recovery machine based on drum elastic tooth film lifting mechanism. *J. Gansu Agric. Univ.* **2022**, *57*, 230–239. (In Chinese) [CrossRef]
6. Kang, J.M.; Wang, S.G.; Yan, L.M.; Wang, N.N.; Di, M.L.; Du, J.W. Design and Experiment of Loosen Shovel Installed on Plastic Film Collecting Machine. *Trans. Chin. Soc. Agric. Mach.* **2016**, *47* (Suppl. S1), 143–148. Available online: https://kns.cnki.net/kcms2/article/abstract?v=3-fZNjprSaw4_41fTY3pr2ZhMppkocKSxAK_ZVnnLE_QPTwryN1Jv-8w4GkLUl7MsKVb6sTv8nq3RZ0lNx1Ft5AnGR3N8U-nQy7LKKSImKg49A0QoQeBVFBUywPolTUoJjLalL-INUtijEILThm2rsRrK632YsOeDK3SrI812JL1Nr1HwIBA6Q==&uniplatform=NZKPT&language=CHS (accessed on 21 October 2025). (In Chinese)
7. Yang, S.M.; Chen, X.G.; Yan, L.M. Performance of three different spades for residual plastic film recycling machine. *Appl. Eng. Agric.* **2020**, *36*, 187–195. [CrossRef]

8. Dai, B.G.; Chen, W.G.; Li, Z.Y.; Zhang, Y.; Yang, X.D.; Zhang, J.H. Research progress on the characteristics of bionic impedance reduction wear on the surface of agricultural earth-touching macthines. *J. Chin. Agric. Mech.* **2025**, *46*, 45–53. [CrossRef]
9. Wang, J.; Wen, N.; Liu, Z.; Zhou, W.; Tang, H.; Wang, Q.; Wang, J. Coupled Bionic Design of Liquid Fertilizer Deep Application Type Opener Based on Sturgeon Streamline to Enhance Opening Performance in Cold Soils of Northeast China. *Agriculture* **2022**, *12*, 615. [CrossRef]
10. Li, J.W.; Gu, T.L.; Chen, X.G.; Li, T.X.; Wang, Z.J.; Hu, B.; Ma, Y.H. Analysis and experiment of the bionic drag reduction characteristics of potato digging shovels on clayey black soil conditions. *Trans. Chin. Soc. Agric. Eng.* **2023**, *39*, 1–9. (In Chinese) [CrossRef]
11. Duo, A. The situation and prevention and control measures in the nursery base in Altay region. *Trans. Chin. Soc. Mod. Gard.* **2015**, *18*, 68. (In Chinese) [CrossRef]
12. Zhang, Y.; Wu, X.L.; Zhu, J.K.; Yuan, J.X. Control technology of mole cricket in forest nursery. *Trans. Chin. Soc. Agric. Sci. Technol. Inf.* **2014**, *13*, 15–24. (In Chinese) [CrossRef]
13. Xiao, M.H.; Wang, K.X.; Yang, W.; Wang, W.C.; Jiang, F. Design and Experiment of Bionic Rotary Blade Based on Claw Toe of Gryllotalpa orientalis Burmeister. *Trans. Chin. Soc. Agric. Mach.* **2021**, *52*, 55–63. [CrossRef]
14. Zhang, Y.; Qiao, C.X.; Wang, T.Q.; Cao, J.F.; Wang, P.F.; Shi, L. Drag reduction mechanism of the 3D geometry of foreleg's claw toe of the mole cricket (Gryllotalpa orientalis). *Trans. Chin. Soc. Agric. Eng.* **2021**, *37*, 309–315. (In Chinese) [CrossRef]
15. Zhang, J.X.; Zhang, K.K.; Zhang, Y.; Zhu, Y.Y. Design of a Soil-Digging Mechanism Based on the Motion Characteristics of Mole Crickets. *Mach. Des. Manuf.* **2020**, *2*, 180–183+187. [CrossRef]
16. Wang, X.Y.; Pan, R.; Qiang, H.; Zhang, Z.H.; Wu, S.H.; Xue, Z. Design and exprement of bionic geometric structure surface on the tip of subsoiler. *Trans. Chin. Soc. Agric. Mech.* **2022**, *43*, 1–6. (In Chinese) [CrossRef]
17. Zhang, G.D.; Qiao, G.B.; Tong, J.J.; Zang, Z.H. Development of device for bionic sub-soil liquid fertilizer. *Trans. Chin. Soc. Agric. Eng.* **2019**, *35*, 29–36. (In Chinese) [CrossRef]
18. Wang, H.T.; Sun, W.; Wang, J.X.; Zhao, M.Y.; Li, Z.Y.; He, Z.X.; Ghen, Z.L.; Xie, Y.Y. Design and research of bionic digging shovel for rhizome Chinese herbal medicine. *J. Gansu Agric. Univ.* **2023**, *58*, 243–250. (In Chinese) [CrossRef]
19. Yang, S.M. Design and Key Technology Research of Passive Cotton Field Residual Plastic Film Recycling Machine. Ph.D.Thesis, Jilin University, Changchun, China, 2020. (In Chinese). [CrossRef]
20. Hong, J.; Xie, J.H.; Ma, W.B.; Zhang, Y.; Shi, Z.L.; Zhao, Y.Y. Design and experiment of profiling mechanism. *Trans. Chin. Soc. J. Agric. Mech. Res.* **2023**, *45*, 211–215. (In Chinese) [CrossRef]
21. Xing, H.H. The Simulation of the Mechanical Excavator Working Resistance Based on Discrete Element Method. Master's Thesis, Dongbei University, Shenyang, China, 2014. (In Chinese).
22. Zhang, Z.P.; Tao, G.X.; Yi, S.J.; Bao, Y.H. Design and finite element analysis of digging shovel of isatis root harvester. *Trans. Chin. Soc. J. Agric. Mech. Res.* **2020**, *42*, 39–45. (In Chinese) [CrossRef]
23. You, J.H.; Zhang, B.H.; Wen, H.J.; Kang, J.M.; Song, Y.Q.; Chen, X.G. Design and Test Optimization on Spade and Tine Combined Residual Plastic Film Device. *Trans. Chin. Soc. Agric. Mach.* **2017**, *48*, 97–104. [CrossRef]
24. Zhang, J.X.; Wang, X.N.; Zhang, L.; Yu, C.; Jiang, Y.X.; Zhang, H.C.; Liu, X.F.; Qiao, Y.Y.; Wang, X.J.; Zhang, S.S.; et al. Effects of mechanical tensile properties of plastic film on plastic recycling method. *Trans. Chin. Soc. Agric. Eng.* **2015**, *31*, 41–47. [CrossRef]
25. Shen, S.L.; Zhang, J.X.; Jiang, Y.X.; Wang, Y.C.; Liu, X.F.; Li, J.M.; Dong, W.H. Tensile Properties of Residual Film in Tillage Layer Based on Discrete Element Method. *Trans. Chin. Soc. Agric. Mach.* **2024**, *55*, 132–141. (In Chinese)
26. Fang, X.; Jin, W.; Zhang, X.J.; Luo, K. Testing and analysis of mechanical properties of agricultural ground membrane. *Trans. Chin. Soc. J. Agric. Mech. Res.* **2019**, *41*, 203–207. (In Chinese) [CrossRef]
27. Jin, W.T.; Wang, S.Y.; Qian, H.F.; Li, W.L.; Yang, J.H.; Ma, L.X. Simulation and experiment of peanut ovary stem removal device based on EDEM. *Trans. Chin. Soc. J. Agric. Mech. Res.* **2023**, *45*, 203–209. (In Chinese) [CrossRef]
28. Zhang, X.J.; Guo, L.; Shi, Z.L.; Yan, J.S.; Liu, X.P.; Zhang, C.S.; Liu, L. Structural optimization and test of the roll type tillage residual film recovery components using FEM-SPH coupling. *Trans. Chin. Soc. Agric. Eng.* **2024**, *40*, 55–65. (In Chinese) [CrossRef]
29. Guo, J.X.; Liu, Y.C.; Wei, Y.J.; Zhou, J.; Shi, Y. Vibration characteristics analysis of the optimal structure of integrated straw returning and residual film recycling machine. *Trans. Chin. Soc. Agric. Eng.* **2024**, *40*, 155–163. (In Chinese) [CrossRef]
30. Liu, H.J.; Yan, W.; Ji, Y.; Zhou, J.; Zhang, W.Y. Working Performance of the Low-Adhesion and Anti-Slip Bionic Press Roller in the Rice–Wheat Rotation Area. *Agriculture* **2022**, *12*, 750. [CrossRef]
31. Xie, K.T.; Zhang, Z.G.; Wang, C.Y.; Tang, J.X.; Yu, X.L. Simulation analysis and test of Panax notoginseng excavating shovel based on LS-DYNA. *Trans. Chin. Soc. J. Northeast. Agric. Univ.* **2021**, *52*, 79–88. (In Chinese) [CrossRef]

32. Zhou, X.C.; Zhang, X.J.; Shi, Z.L.; Zhang, C.S.; Bai, S.H.; Bai, S.H. Design and test of film lifting separation conveying device of stripper-plate-type residual film recovery machine. *Trans. Chin. Soc. J. Shihezi Univ. (Nat. Sci.)* **2022**, *40*, 472–480. (In Chinese) [CrossRef]
33. Jiang, Y.X.; Qu, H.; Liu, X.F.; Zhang, H.C.; Zhou, X.; Zhang, L. Design and Experiment of Spade Tooth Film Lifting Device for Residual Film Recycling Machine. *Trans. Chin. Soc. Agric. Mach.* **2025**, *56*, 282–289. [CrossRef]

Disclaimer/Publisher's Note: The statements, opinions and data contained in all publications are solely those of the individual author(s) and contributor(s) and not of MDPI and/or the editor(s). MDPI and/or the editor(s) disclaim responsibility for any injury to people or property resulting from any ideas, methods, instructions or products referred to in the content.